Photometric analysis of WASP-135b with TASTE and TESS data

P. Bussatori[1] and L. Nardo[1]

Department of Physics and Astronomy, University of Padua, Vicolo Osservatorio, 3, 35122, Padua
e-mail:
patrizia.bussatori@studenti.unipd.it
linda.nardo@studenti.unipd.it

ABSTRACT

Context. In this paper we present the analysis performed on the confirmed hot Jupiter WASP-135b transiting a G5V-type star with mass $0.980 \pm 0.060\ M_\odot$ at a distance of 298 *pc*.
Aims. The goal is to retrieve the main parameters of WASP-135b, such as period, radius, impact parameter, inclination and semi-major axis of the orbit using observations obtained with the ground-based TASTE survey from Asiago (Italy) and the TESS Space Telescope.
Methods. For TASTE, we calibrated the data and extracted the differential aperture photometry flux, normalised to a reference star present in the same FOV. For TESS, the data set was already calibrated by the Science Processing and Operations Center (SPOC) and available in the MAST archive. The Pre-search Data Conditioning Simple Aperture Photometry (PDCSAP) light curve had to be flattened, to remove possible stellar trends while preserving the transit signal. In order to do so, we used Python package Wōtan, which provides different detrending models. The most suitable for this particular case was Tukey's *biweight* estimator. Finally, we executed Python tool PyORBIT on TESS and TASTE data separately to acquire the physical parameters of the source.
Results. We obtained a value for the radius of $1.246^{+0.069}_{-0.067}\ R_J$ and $1.292 \pm 0.069\ R_J$ for TESS and TASTE respectively and a period of 1.401377 ± 0.000001 days for both.

Key words. techniques: transits – star: WASP-135 – planets: WASP-135b

1. Introduction

The existence of planets outside the Solar System was assumed for many years and the first hints of planetary companions were reported in the 80s. However, the first confirmed discovery occurred thanks to the radial velocity technique in 1995, when Michel Mayor and Didier Queloz (Mayor & Queloz 1995) observed 51 Peg b, orbiting a G5IV star at 0.052 *AU* and with a possible minimum mass of 0.46 M_J. Up to now, 5250 exoplanets have been discovered[1], the vast majority with the transit technique. There are many different kinds of methods to find and characterize exoplanets, but the transit, combined with the radial velocity measurements, allows a complete characterization of the planet and of the planetary system itself.

The concept at the basis of the transit technique is quite simple and consists in the measurement of the stellar flux reduction due to the transit of the planet in front of (or behind) the stellar disk. This allows to reconstruct the phase light curve, showing the flux (or the normalized flux) as a function of the planet phase. The largest flux decrement occurs in case of a transit, while for an occultation the reduction of the intensity is smaller: in both configurations we receive less photons by the hosting star, because in the first case the planet is in front of the stellar disk, obstructing the part of the radiation, while during a secondary eclipse we observe only the stellar flux, without any contribution from the planet. As explained by Winn 2010, the transit method is a photometric technique useful for the estimation of the planet radius by applying the relation $\Delta F/F = (R_p/R_\star)^2$: the stellar radius $R_\star$ can be assumed from theoretical models, the

stellar flux F can be estimated knowing the spectral type and ΔF is measured from the light curve. In this way, it is possible to compute the planet radius R_p. From the relation above, it is clear that this approach is more suitable for systems with smaller stars and bigger exoplanets, like gaseous giants. As consequence, this method introduces several observational biases, but on the other hand it is very powerful for the transmission spectroscopy technique, which allows the study of exoplanetary atmospheres.

With this knowledge, this work reports the analysis of the transit of a known exoplanet, the hot Jupiter WASP-135b, orbiting WASP-135 (1SWASPJ174908.40+295244.9), a G5V-type star. Hints of its existence were found previously by Cutri et al. 2003 and later by Collier Cameron et al. 2006, thanks to a fast hybrid algorithm for exoplanetary transit search, developed at the time for the WASP survey. The official discovery occurred only ten years later by Spake et al. 2016, who conducted an entire study on the planet and its hosting star using transit and radial velocity methods.

The paper is structured as follows. In the current Section we provided an introduction on the discovery of exoplanets and in particular on the transit method. In Section 2 we report the stellar parameters of WASP-135 inferred by Spake et al. 2016. In Section 3 we describe TASTE observations, data calibration and light curve extraction. In Section 4 we describe TESS observations and light curve extraction. In Section 5 we present the data analysis performed with PyORBIT, and finally, in Section 6, we sum up our results and draw the conclusions.

---

[1] https://exoplanetarchive.ipac.caltech.edu/

2. Stellar Parameters

WASP-135 is a G5V-type star, located at a distance of $298.214^{+1.420}_{-1.407}$ pc with coordinates RA 17h 49m 08.40s Dec +29d 52m 44.55s. Its apparent magnitude is $m_V = 13.181 \pm 0.080$ in V band and $m_{TESS} = 12.4197 \pm 0.0069$ in TESS band (Cutri et al. 2003, Gaia Collaboration et al. 2018 and Stassun et al. 2019).

In order to compute the features of the exoplanet, the first fundamental step is to retrieve the stellar parameters from an independent spectroscopic analysis, which in this case is based on the work of Spake et al. 2016. Stellar parameters were obtained with SOPHIE, the cross-dispersed échelle spectrograph at the Haute-Provence Observatory, located in south-eastern France. The results are listed in Table 1 and have been used as priors in the final analysis with PyORBIT (Malavolta et al. 2016, Malavolta et al. 2018). Another important parameter, especially to gain a deeper understanding of the planetary system formation and evolution, is the stellar age, even though it is also one of the most difficult to obtain. Sestito & Randich 2005 give an estimation of about $0.60^{+1.40}_{-0.35}$ Gyr.

We considered also the limb darkening effect, that causes the gradual decrease in brightness of a star from the central region to its edge, or limb, because the optical depth assumes lower values from the center (where it is infinite) towards the borders, due to the presence of thinner gaseous layers. As a consequence, this effect depends on the wavelength of observation and it is more relevant for blue light, for which the difference in brightness between the center and in the outer regions is about 90%. This issue can be treated by modelling the effect with many different fitting functions, so that it can be taken it into consideration during the data analysis. For our work, we chose a quadratic function and estimated the limb darkening coefficients with associated errors, which may be, however, underestimated, since they don't take into account errors in theoretical model atmospheres.

Table 1. Stellar parameters from spectroscopic analysis.

Parameter	Value
$M_\star$ ($M_\odot$)	0.980 ± 0.060
$R_\star$ ($R_\odot$)	0.960 ± 0.050
$\rho_\star$ ($\rho_\odot$)	1.120 ± 0.150
$\log(g)$ (cgs)	4.47 ± 0.03
T_{eff} (K)	5675 ± 60

3. TASTE

The Asiago Survey for Timing transit variations of Exoplanets (TASTE) is a collection of high-precision, short-cadence light curves for a selected sample of transits, retrieved by using imaging differential photometry at the Asiago 1.82 m Copernico telescope (Nascimbeni et al. 2011). We analysed the data collected on March 12, 2021, with an exposure time of 5 s, using the Sloan r filter. The raw data contained 1928 science frames, which had to be corrected for bias and flat-field (30 frames each), in order to account for any instrumental error.

Times were expressed in Julian Date units (JD) so, as first thing, we had to perform a conversion into Barycentric Julian Date (BJD), to center the frame of reference in the barycenter
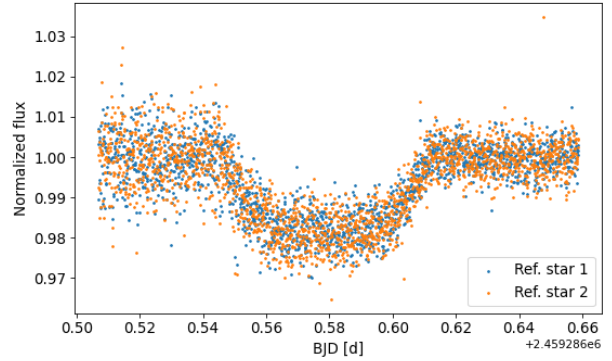
Fig. 1. Comparison of the light curves obtained with two different reference stars.

of the Solar System. Moreover, the target coordinates retrieved from the SIMBAD astronomical database[2] (Wenger et al. 2000) had to be shifted to the International Celestial Reference System (ICRS), which returns the coordinates of the object with respect to the barycenter of the Solar System. This allowed the computation of the *light travel time* correction (the time required by the light to travel between Earth and the Solar System barycenter), that, when summed to the JD, returns the times in BJD units.

3.1. Differential aperture photometry

To identify the target star in the corrected science frames, we made use of the SIMBAD database. To perform the differential aperture photometry, which consists in comparing a source of interest to other sources present on the same frames to reduce any kind of residual noise it may contain, the target star was selected with a circle to include its flux and it was then corrected by the background contribution, estimated by choosing an outer concentric annulus to form a circular crown around the star, from which we extracted the sky flux. The same procedure has been applied to two reference stars, whose fluxes were used to normalise the target flux (F_{target}/F_{ref}) and obtain the differential aperture photometry light curve. To convert these results into a common scale and allow a comparison, both of them were normalised with polynomial functions (Fig. 1). With this procedure, we were able to state that the first reference star produces less scattered data points, which means it is more suitable for the computation of the final light curve. Moreover, we checked that the position of target remained the same by comparing its coordinates in all frames with their median and plotting its dislocation along the x and y axes, but no peculiar trends were found. Target and reference star fluxes as function of time are shown in Fig. 2 while their associated errors are reported in Fig. 9.

4. TESS

The *Transiting Exoplanet Survey Satellite* (TESS, Ricker et al. 2015) is a space mission launched by NASA in April 2018 with the goal of discovering new exoplanets using the transit method. The satellite is equipped with 4 wide-field CCD cameras that can scan a different region of the sky measuring $24° \times 96°$ every two orbits around Earth (~ 27 days). The cameras produce two-minute stacked subarrays and 30-minute Full-Frame Images (FFIs). The two-minute subarrays are centered on stars with the
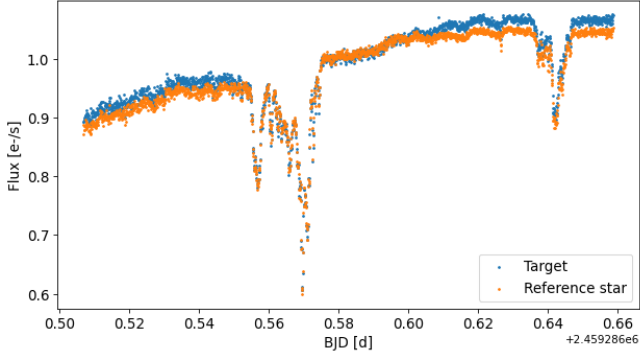
---

[2] https://simbad.u-strasbg.fr/simbad/

Fig. 2. Target and reference star fluxes as function of time. The drops of intensity are due to the sky flux correction.

potential for exoplanet discovery, while the FFIs can be examined for transiting planets around targets not specified in the two-minute data set (Vanderspek et al. 2018).

Before release, the raw data are calibrated by the Science Processing and Operations Center (SPOC) Vanderspek, Doty, Fausnaugh et al. nas. The SPOC pipeline processes the raw pixels, extracts photometry and astrometry for each target star, identifies and removes systematic errors and performs a suite of diagnostic tests. Through the ExoFOP (*Exoplanet Follow-up Observing Program*) website[3], we were able to find the sector numbers in which the target was observed, so that we could retrieve the data in the Mikulski Archive for Space Telescopes (MAST)[4]. In this specific case, the interested sectors are 26 (Fausnaugh et al. 2020) and 52 (Fausnaugh et al. 2022), whose main observational information are reported in Table 2. There is a huge time difference of about 2 years between the two set of observations, which resulted as a tricky point in the data analysis step made with the PyORBIT.

Table 2. TESS sectors in which the target has been observed.

TESS sectors		
26		
Start	2020-06-09 T18:28:14.221	UTC
End	2020-07-04 T15:18:03.377	UTC
Exposure	19.6954	*d* on the source
52		
Start	2022-05-19 T03:17:14.068	UTC
End	2022-06-12 T13:53:49.012	UTC
Exposure	19.3581	*d* on the source

In the folders downloaded from the MAST Archive (one per each sector) there are two main files, containing the Target Pixel File (TPF) and the light curves respectively. The following analysis concerns only the latter, which includes two different kinds of light curves: the Simple Aperture Photometry (SAP) light curve and the Pre-search Data Conditioning SAP (PDC-SAP) light curve. The SAP flux is obtained after summing the
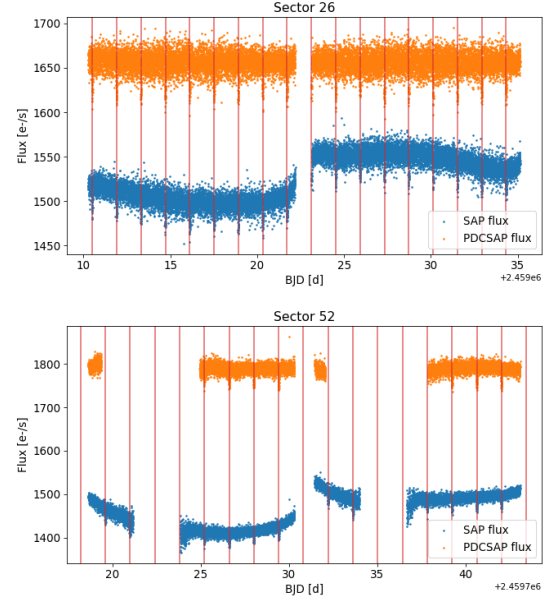
Fig. 3. SAP and PDCSAP fluxes for both sectors. Vertical red lines indicate the transit of the planet.

calibrated pixels within the TESS optimal photometric aperture. Of course, the choice of the aperture mask is a fundamental step to avoid nearby contamination and improve the strength of the specific background signal. The PDCSAP flux is the SAP flux value nominally corrected for instrumental variations. Thus, it is the mission's best estimate of the intrinsic variability of the target and it has been pre-generated using NASA's Data Processing Pipeline. PDCSAP flux is usually cleaner than the SAP flux and will have fewer systematic trends.

Times are in TESS Julian Date (TJD) units, which means they are all offset by a value of 2457000, stored in the header under BJDREFI, so, as first thing, we had to correct the data for this quantity. Next, we visualised SAP and PDCSAP fluxes of both sectors (Fig. 3): the holes in the plots are due to the fact that, at the end of each orbit, observations are stopped for approximately 16 hours for data downlink to the ground stations. Sector 52 shows additional empty regions, probably due to mechanical and electronic issues or simply to a specific schedule of observations.

All data points in the PDCSAP flux with quality flags different from 0 were excluded from the analysis, because affected by systematic errors from the telescope[5].

4.1. Light curve flattening

After these first considerations, the PDCSAP light curve needs to be *flattened*, which means performing an additional correction to remove stellar trends while preserving transit signals. With this intention, two different detrending methods from the open source Python package Wōtan have been tested (Hippke et al. 2019): Tukey's *biweight* estimator and the *Huber spline*.

– The *biweight* estimator works by first computing a preliminary estimate of the mean flux, and then weighting each data point based on its deviation from this value (only those points
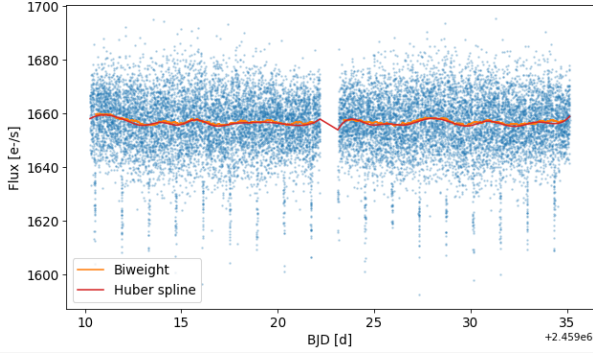
Fig. 4. Comparison between Tukey's *biweight* estimator and the *Huber spline* in Sector 26.

Fig. 5. Periodogram for Sector 26.

Fig. 6. Light curve fit with TLS for Sector 26.

laying within a certain range of flux are considered by the algorithm). The final estimate is obtained by taking a weighted average of the data points, where the weights are determined by Tukey's *biweight* function;

– The *Huber spline* is a robust version of the least squares estimator and it down-weights the influence of outliers in the data. In this method, the light curve is divided into segments and the Huber estimator is used to evaluate the coefficients of the polynomials to fit each segment. The best result minimizes the sum of weighted squared deviations between the data points and the polynomial.

A graphic comparison of the two models for Sector 26 is shown in Fig. 4, while the resulting standard deviations are reported in Table 3. The *Huber spline* performs well, but the *biweight* estimator gives a slightly lower STD value, therefore we used it to flatten the PDCSAP light curve.

Table 3. Comparison between detrending methods. STD of normalised PDCSAP light curve is also reported for completeness.

Sector 26	
PDCSAP STD	0.00593
Biweight STD	0.00590
Huber STD	0.00591
Sector 52	
PDCSAP STD	0.00475
Biweight STD	0.00467
Huber STD	0.00469

Finally, we analysed the flattened light curve with two different algorithms able to roughly reproduce the transits, using as parameters depth, width, phase and period: the Box-fitting Least Square (BLS), which approximates the flux decrement to a box, and the Transit Least Square (TLS), an actual transit shape which accounts also for the effects that can smooth the transit curve. The different results for BLS are visualised in a periodogram, a plot relating different choices of periods between subsequent transits and a quantity called Signal Residue (SR), which allows to state the quality of the model (the original periodogram analyses the frequency of the transits, but in this situation it makes more sense working with periods). The
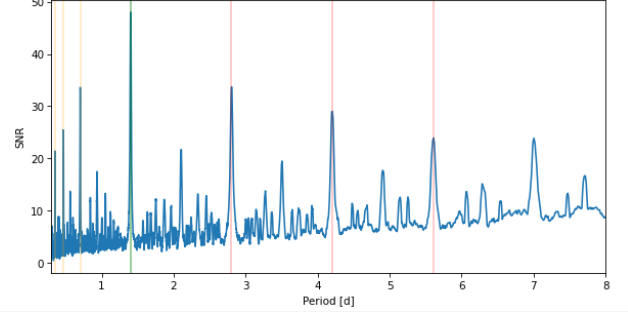
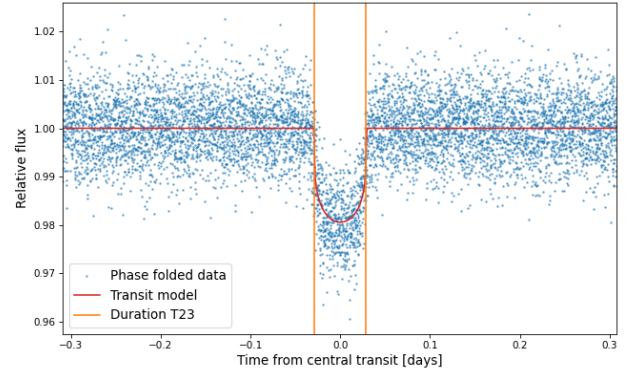solution is identified by the largest peak (Fig. 5) and it allows to obtain some preliminary results to use as initialization parameters in the final step performed by `PyORBIT`, which in this case are the period $P = 1.4007$ days and central time of the transit $T_c = 2459011.9111$ *BJD*. Furthermore, we're already able to visualize the folded light curve, that displays the average brightness of the object as a function of the phase (the fraction of the period that has elapsed since the reference time). Similar outcomes are obtained with TLS, which results in an improved Signal Detection Efficiency (SDE, equivalent to SR but with a different metric; both return the inverse of the χ^2). In Fig. 6 we can see the light curve fit with TLS for Sector 26 as example.

5. Data analysis

To compute the data analysis we used `PyORBIT`, a powerful Python code to acquire exoplanet orbital parameters and information on stellar activity (Malavolta et al. 2016, Malavolta et al. 2018). It is a versatile framework to study planetary systems performing both Markov Chain Monte-Carlo and Bayesian statistics algorithms to model phase light curves, radial velocity curves, activity indices and transit time variations. As input it receives a `.yaml` file containing priors and intervals within which the algorithm will search for an optimal solution. The output files contain the final estimation of physical and fitting parameters. According to our research goal, we operated only with phase light curve modelling. The stellar parameters described in Section 2 and reported in Table 1 have been used as priors to fit both TASTE and TESS observations.

5.1. TESS data analysis

The input file is the flattened PDCSAP flux obtained in Section 4. As said before, the two TESS sectors in which WASP-135 was observed are really distant one from the other in terms of time (more than 700 days), making it harder for the algorithm to converge to an optimal solution. As consequence, we set smaller intervals around the priors of period ($P = 1.4007 \pm 0.05$) and central time of the transit ($T_c = 2459011.9111 \pm 0.05\ BJD$). We assumed circular orbits and fixed Gaussian priors for the stellar parameters. For the limb darkening effect, a quadratic law was assumed without any prior on the coefficients. Furthermore, we took into account that the propagation of errors from the first sector to the second one introduces a relevant offset in the fitting procedure due to the time difference, therefore we decided to model the data generating 200000 points instead of 50000 suggested by default. Once completed the `.yaml` with this setup, we executed `PyORBIT`.

The outcome is contained in Table 4 and is a complete statistics on the physical parameters. Let us highlight some values: the orbital period $P = 1.401377 \pm 0.000001$ days; the central time of the transit $T_c = 2459011.9092 \pm 0.0003\ BJD$; the inclination of the orbital plane with respect to the plane tangential to the celestial sphere $i = 82.619^{+0.451\circ}_{-0.417}$; the radius $R_p = 1.292 \pm 0.069\ R_J$; the semi-major axes of the orbit $a = 0.025 \pm 0.001\ AU$. Correlations between these parameters can be appreciated in the corner plot (Fig. 10) of Section 7.

Through the results obtained by the statistics computed by `PyORBIT` we fitted the observations with a model to retrieve the light curve generated by the planet transiting in front of the hosting star. The final plot is shown in Fig. 7. In the upper diagram we can see the normalized flux as function of the orbital phase, where the decrement of ~ 0.02 in the flux intensity is evident. In the lower diagram, residuals of the observation are plotted as function of the orbital phase.

5.2. TASTE data analysis

For the fit of TASTE transit curve we used the differential light curve derived in Section 3. We assumed circular orbits and a polynomial trend for the light curve, while we set as period boundaries a slightly larger range with respect to TESS ($P = 1.4007 \pm 0.1$) and as central time boundaries the extremes of TASTE observation time. We gave an ulterior Gaussian prior for the period, with TESS output as input. Like for TESS, we fixed Gaussian priors for the stellar parameters around the values from the literature and set the limb darkening contribution with a quadratic law, this time giving initial values for the coefficients (Sloan r filter, $LD\ c_1 = 0.6117 \pm 0.0322$ and $LD\ c_2 = 0.1018 \pm 0.0771$, obtained with the Python toolkit by Parviainen & Aigrain 2015). For TASTE we keep the other default parameters.

As before, `PyORBIT` outcome is a complete statistics on the physical parameters obtained from the posterior samples. The main results are: the planetary period $P = 1.401377 \pm 0.000001$ days; the central time of the transit $T_c = 2459286.578 \pm 0.0003\ BJD$; the inclination $i = 83.405^{+0.501\circ}_{-0.489}$; the radius $R_p = 1.246^{+0.069}_{-0.067}\ R_J$ and the semi-major axes of the planet orbit $a = 0.026 \pm 0.002\ AU$. All parameters obtained with TASTE data set are listened in Table 4. Possible correlations between these pa-
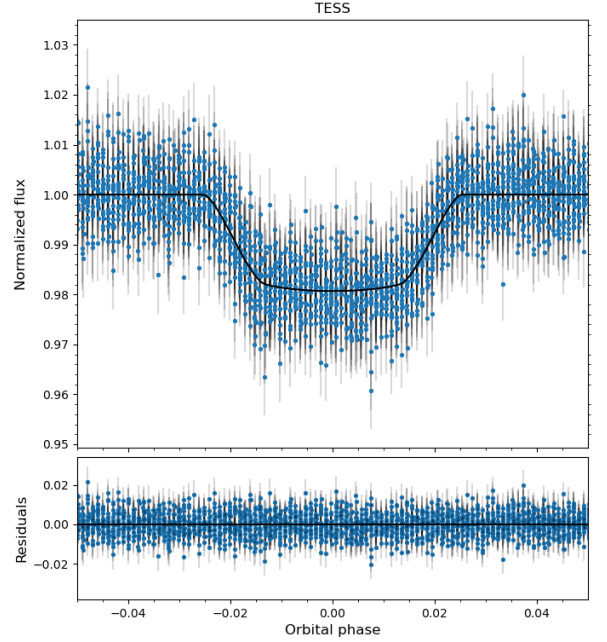

Fig. 7. *Upper plot*: Normalized flux as function of the orbital phase for TESS observations of sectors 26 and 52. *Lower plot*: Residuals of the observations as function of the orbital phase. Error bars are represented by thin gray vertical lines, while the black continuous lines show the models for the light curves and for the residuals respectively.

rameters are reported in the corner plot (Fig.11) in the Section 7.

Based on these values, the model fit of the phase light curve was performed and the final diagram is shown in Fig. 8, where we can observe a decrement ~ 0.02 in the flux intensity due to the transit of the planet in front of the stellar disk. This outcome is consistent with TESS analysis.

6. Conclusions

The aim of this analysis was to study the transit of WASP-135b, a hot Jupiter-like planet, orbiting a G5V-type star, and compare our results with the existing literature. With this purpose, we studied the ground-based observations available in the TASTE survey, along with the ones obtained by the space satellite TESS, which observed the target twice in sectors 26 and 52. We performed a pre-analysis to extract a normalised flattened light curve for both data sets, to give as input to the `PyORBIT` algorithm, along with a certain confidence interval for P and T_c to use as prior. The results are shown in Table 4 and they are all consistent with each other. In particular, the period is exactly the same for both, while the central time of the transit is different because it depends on the date of observation. Furthermore, both orbital inclination and radius of the planet are comparable as well. The semi-major axis are analogous. On the other hand, with respect to Spake et al. 2016, the values of the parameters are very similar but not exactly in agreement, even considering the error bars. Further analysis should be made to investigate this discrepancy.

References

Collier Cameron A., et al., 2006, MNRAS, 373, 799
Cutri R. M., et al., 2003, 2MASS All Sky Catalog of point sources.
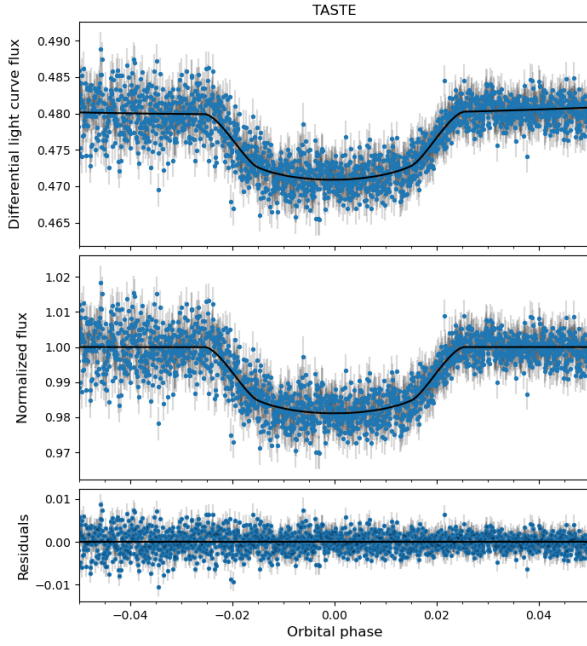
Fig. 8. *Upper plot*: Differential light curve flux as function of the orbital phase. *Middle plot*: Normalized flux as function of the orbital phase. *Lower plot:* Residuals of the observations as function of the orbital phase. Error bars are represented by thin gray vertical lines, while the black continuous lines show the models for the light curves and for the residuals respectively.

Fausnaugh M. M., et al., 2020
Fausnaugh M. M., et al., 2022
Gaia Collaboration et al., 2018, A&A, 616, A1
Hippke M., David T. J., Mulders G. D., Heller R., 2019, AJ, 158, 143
Malavolta L., et al., 2016, Astronomy &amp$$ Astrophysics, 588, A118
Malavolta L., et al., 2018, The Astronomical Journal, 155, 107
Mayor M., Queloz D., 1995, Nature, 378, 355
Nascimbeni V., Piotto G., Bedin L., Damasso M., 2011, A&A, 527, A85
Parviainen H., Aigrain S., 2015, MNRAS, 453, 3821
Ricker G. R., et al., 2015, Journal of Astronomical Telescopes, Instruments, and Systems, 1, 014003
Sestito P., Randich S., 2005, A&A, 442, 615
Spake J. J., et al., 2016, PASP, 128, 024401
Stassun K. G., et al., 2019, AJ, 158, 138
Vanderspek R., Doty J., Fausnaugh M., et al., 2018, TESS Instrument Handbook, v0. 1, Mikulski Archive for Space Telescopes
Wenger M., et al., 2000, Astronomy and Astrophysics Supplement Series, 143, 9
Winn J. N., 2010, Transits and Occultations, doi:10.48550/ARXIV.1001.2010, https://arxiv.org/abs/1001.2010
Tess Science Support Center, https://heasarc.gsfc.nasa.gov/docs/tess/pipeline.html

7. Extra materials

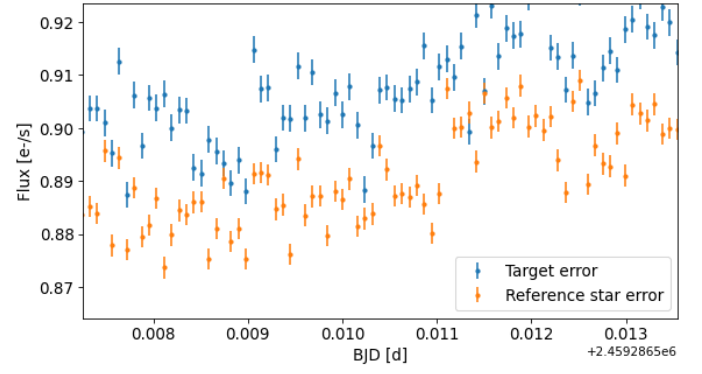We would like to include some extra materials for a better and clearer understanding.

Fig. 9. A zoom in of a portion of TASTE data to appreciate the associated error bars.

Table 4. PyORBIT results on TESS and TASTE data: b is the impact parameter, $LD\ c_1$ e $LD\ c_2$ are the limb darkening coefficients, T_{41} is the interval time between first and last external conjunctions of the planet with the stellar disk and T_{32} is the interval time between first and last internal conjunctions.

| Parameter	TESS values	TASTE values
$P\ (d)$	1.401377 ± 0.000001	1.401377 ± 0.000001
$T_c\ (BJD)$	2459286.5784 ± 0.0002	2459011.9092 ± 0.0003
b	$0.667^{+0.030}_{-0.034}$	$0.722^{+0.022}_{-0.028}$
$\rho_\star\ (\rho_\odot)$	$1.339^{+0.117}_{-0.110}$	$1.213^{+0.102}_{-0.091}$
$LD\ c_1$	$0.599^{+0.031}_{-0.032}$	$0.214^{+0.234}_{-0.154}$
$LD\ c_2$	$0.058^{+0.078}_{-0.076}$	$0.088^{+0.271}_{-0.209}$
$i\ (°)$	$83.405^{+0.501}_{-0.489}$	$82.619^{+0.451}_{-0.417}$
$R_p\ (R_J)$	$1.246^{+0.069}_{-0.067}$	1.292 ± 0.069
$R_p\ (R_e)$	$13.967^{+0.768}_{-0.756}$	$14.478^{+0.772}_{-0.770}$
$T_{41}\ (d)$	0.071 ± 0.001	0.071 ± 0.001
$T_{32}\ (d)$	0.043 ± 0.002	$0.038^{+0.003}_{-0.002}$
$a\ (AU)$	0.026 ± 0.002	0.025 ± 0.001
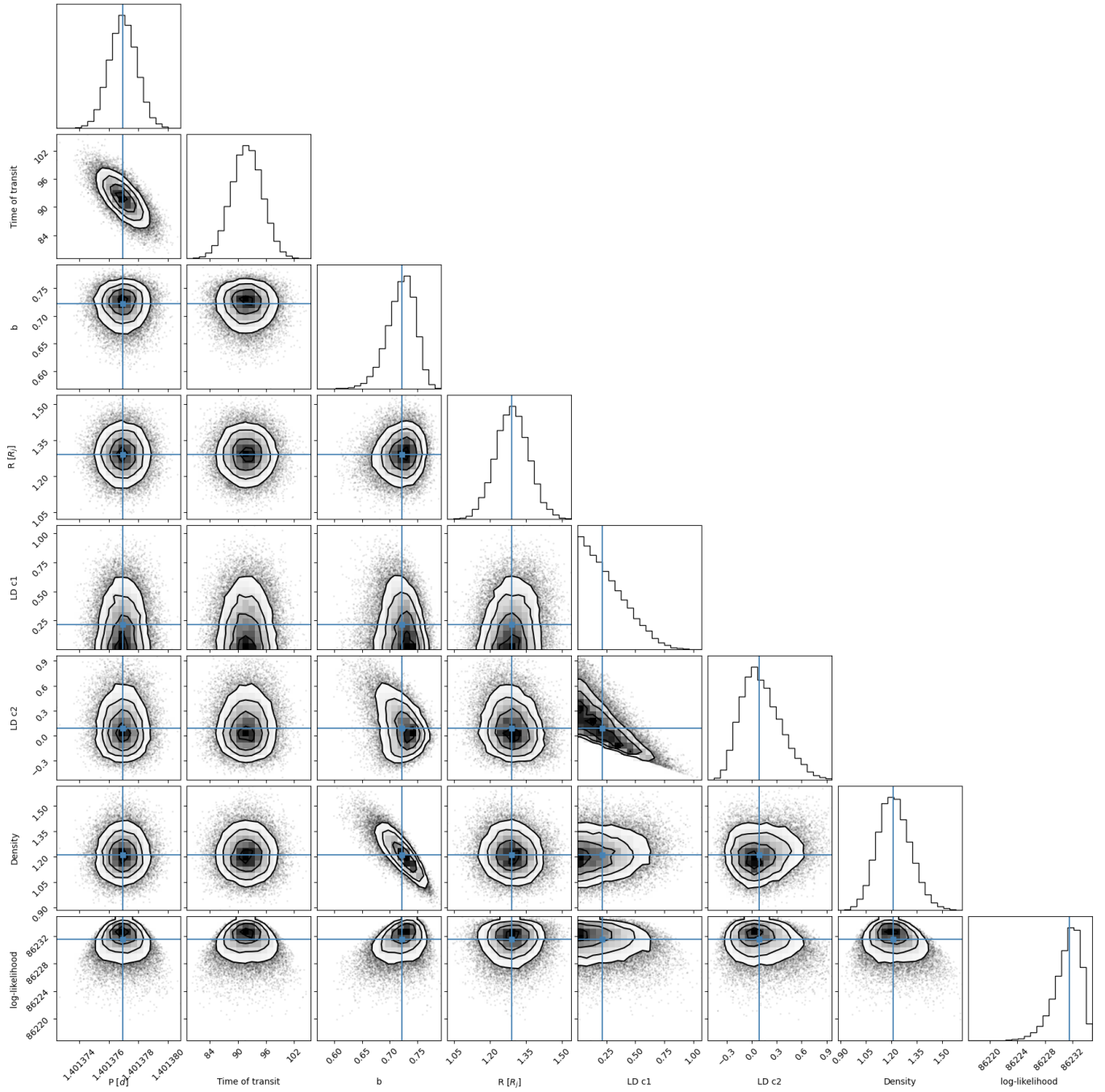
Fig. 10. Corner plot from TESS analysis.
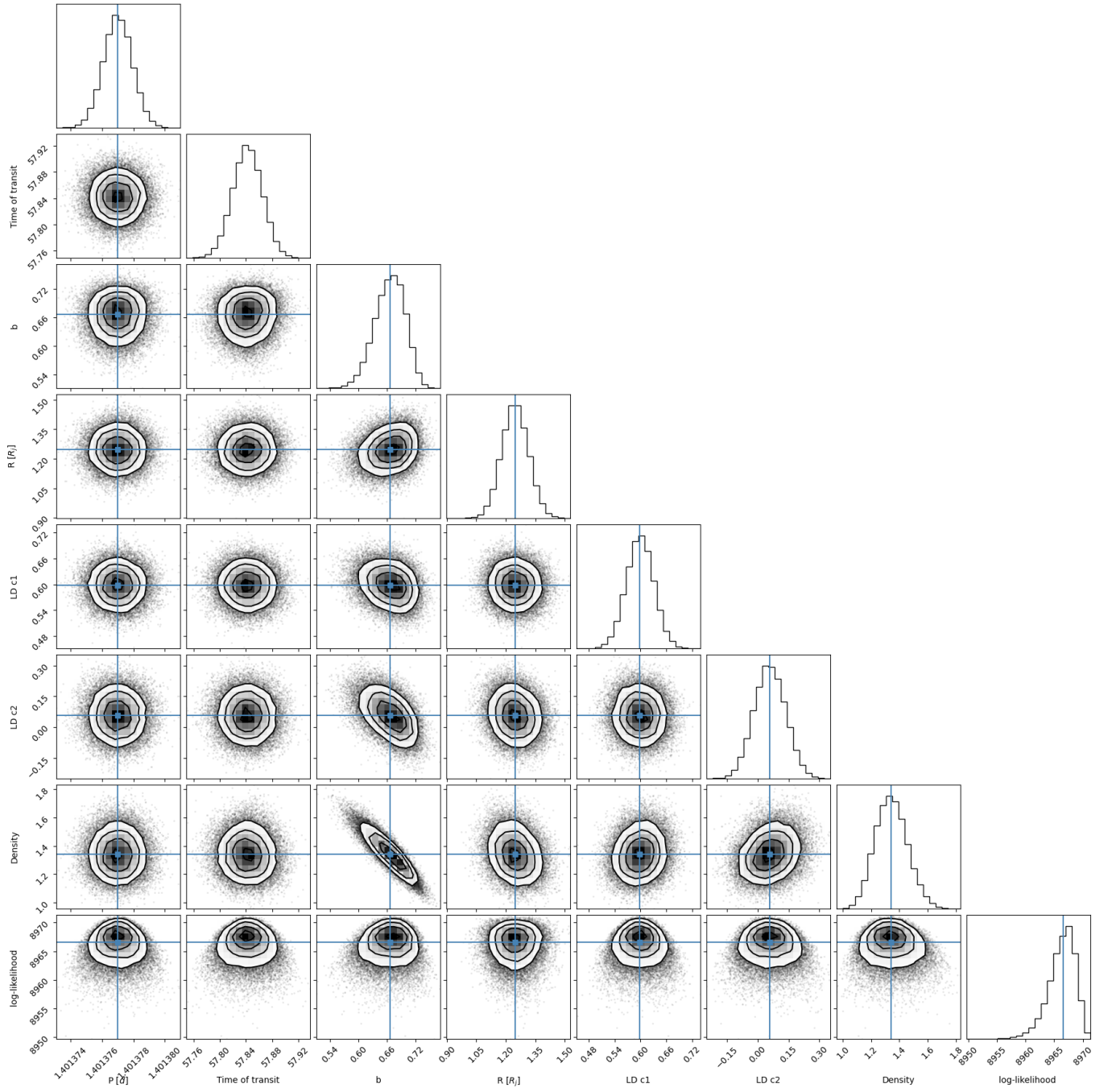
Fig. 11. Corner plot from TASTE analysis.